Article:
Faranda, D., Zanchi, M., Yiou, P. et al. (2026) Conditional attribution and socioeconomic exposure of the March 2026 North America early heatwave. Environmental Research Letters, 21 (14). 144006. ISSN: 1748-9318

https://doi.org/10.1088/1748-9326/ae870d

ENVIRONMENTAL RESEARCH
LETTERS

LETTER • OPEN ACCESS

Conditional attribution and socioeconomic exposure of the March 2026 North America early heatwave

To cite this article: Davide Faranda *et al* 2026 *Environ. Res. Lett.* **21** 144006

ENVIRONMENTAL RESEARCH
LETTERS

Check for updates

OPEN ACCESS

RECEIVED
3 April 2026

REVISED
8 June 2026

ACCEPTED FOR PUBLICATION
7 July 2026

PUBLISHED
14 July 2026

LETTER

Conditional attribution and socioeconomic exposure of the March 2026 North America early heatwave

Davide Faranda[1,2,3,9,*], **Marco Zanchi**[1,9], **Pascal Yiou**[1], **Marco Chericoni**[4], **Mathieu Vrac**[1], **Haosu Tang**[5], **Stavros Dafis**[6], **Gianmarco Mengaldo**[7] **and Tommaso Alberti**[8]

1 Laboratoire des Sciences du Climat et de l'Environnement (LSCE/IPSL), CNRS, Université Paris-Saclay, Gif-sur-Yvette, France
2 Laboratoire de Météorologie Dynamique (LMD/IPSL), École Normale Supérieure, Ecole Polytechnique, PSL Research University, Paris-Palaiseau, France
3 London Mathematical Laboratory, London, United Kingdom
4 CMCC Foundation—Euro-Mediterranean Center on Climate Change, Bologna, Italy
5 School of Geography and Planning, University of Sheffield, Sheffield, United Kingdom
6 National Observatory of Athens, Institute for Environmental Research and Sustainable Development, Athens, Greece
7 National University of Singapore, Singapore, Singapore
8 Istituto Nazionale di Geofisica e Vulcanologia, Rome, Italia
9 These authors contributed equally.
* Author to whom any correspondence should be addressed.

E-mail: davide.faranda@lsce.ipsl.fr

Keywords: attribution, heatwave, climate Dynamics, climate extremes

Supplementary material for this article is available online

Abstract

In March 2026, an intense and spatially extensive heatwave affected a large portion of the North America. Here, we assess the influence of anthropogenic climate change and natural variability on the event using the ClimaMeter analogue-based attribution protocol applied to ERA5 reanalysis. We compare present-day circulation analogues (1988–2025) of March 2026, with analogues from a cooler past climate (1950–1987). We find that events similar to the March 2026 heatwave are associated with near-surface temperatures that are typically 1 °C to 3 °C warmer in the present climate than in the past, with locally larger increases. By looking at natural variability modes, we observe that human-driven climate change substantially amplified the thermal hazard of the event, while natural variability had only a limited influence on the circulation pattern associated with the event. We further integrate the meteorological attribution with an exposure analysis, combining the heat hazard with gridded population and gross domestic product. We find that nearly 50 million people and more than 2.5 trillion USD in economic assets were located in areas where the heat hazard coincided with a statistically significant climate change amplification of temperature. This underscores the growing contribution of anthropogenic climate change to heat risk amplification across the North America.

1. Introduction

Amplified heatwaves are among the most impactful manifestations of ongoing climate change. Across North America, observed warming has increased both the frequency and intensity of hot extremes, and further warming is expected to increase the occurrence, duration and severity of such events [1]. At the regional scale, Central America has experienced consistent warming trends [2], reflecting a climate system in which rising mean temperatures systematically shift the distribution toward more frequent hot extremes [1]. Previous attribution studies have shown that greenhouse gas forcing has increased the likelihood of heatwaves over Mexico and the United States [3, 4]. These regions exhibit strong and consistent warming signals [5], with well-documented increases in the frequency of hot days [6] alongside substantial changes in nighttime temperatures [7].

Recent extreme heat events in North America further highlight this context. The 2021 North American heatwave was an exceptional event, during which temperatures in major western U.S. cities exceeded climatological maxima by 10 °C–20 °C [8]. The event arose from the interaction between slow and fast atmospheric circulation patterns, in combination with pre-existing soil moisture deficits [9], and was further intensified by nonlinear land-atmosphere feedbacks [10]. This heatwave has been extensively investigated [11–13], with studies showing that anthropogenic climate change significantly increased both its likelihood and intensity [14]. Also in 2023, the southwestern United States and northern Mexico experienced a record-long heatwave with major societal and economic impacts, driven by a persistent anticyclonic blocking pattern lasting over six weeks and linked to exceptionally warm Atlantic sea surface temperatures [15]. These results support a framework in which warming and persistent circulation anomalies act jointly, in line with evidence that changes in recurrent weather patterns can intensify regional extremes and amplify long-term warming trends [16].

The societal consequences of heatwaves are also increasing [17]. Heat-related mortality in the North America has risen in several regions [18, 19], in some cases outpacing traditional measures of hazard severity [20]. Exposure is especially important where strong thermal anomalies overlap with densely populated or economically important areas [21, 22]. In addition, early-season heatwaves can produce disproportionate health impacts because populations are not yet physiologically and socially acclimatized to high temperatures [18, 23, 24]. For this reason, integrating physical attribution with an exposure-based perspective provides a more comprehensive understanding of how climate change amplifies not only the hazard itself, but also its potential impacts.

In the second half March 2026, a record-breaking heatwave affected large parts of the North America, with temperatures far exceeding typical early-season values across several regions. The early-season timing of this event makes it particularly noteworthy, as anomalous heat in this period can catch populations and ecosystems unprepared, with potentially severe societal and economic consequences. Rapid assessments, including those performed within the World Weather Attribution framework [25], indicate that such an event would have been extremely unlikely in a pre-industrial climate.

Building on these initial findings, we analyse the March 2026 United States heatwave using the ClimaMeter analogue-based attribution framework [26]. In particular, we focus on three key aspects: (1) the characterization of an exceptionally early-season extreme; (2) the application of an analogue-based rapid attribution framework; and (3) the linkage between the physical hazard and population and economic exposure. We first evaluate how circulation patterns analogous to the event differ between a warmer present climate and a cooler past climate, and how these differences translate into changes in near-surface temperature, precipitation, and wind speed. We then assess whether the large-scale circulation associated with the event is exceptional, both for this time of year and in the context of the full annual variability. Finally, we combine the meteorological attribution with gridded population and gross domestic product (GDP) data to quantify the extent of present-day exposure located in areas where climate change has significantly increased the heat hazard.

2. Data and methods

The methodology follows the ClimaMeter analogue based framework for rapid conditional event attribution, previously described in detail in [26]. In brief, we identify atmospheric analogues of the March 2026 North American heatwave using European Centre for Medium Range Weather Forecasts Reanalysis version 5 (ERA5; [27]) 500 hPa geopotential height anomalies over North America, comparing analogue composites between a past climate (1950 to 1987) and a present climate (1988 to 2025). Composite differences in temperature, precipitation, and circulation fields are interpreted as the thermodynamic contribution of anthropogenic climate change under similar dynamical conditions. Statistical significance is assessed through a bootstrap resampling procedure [28] applied to the analogue sets, while the potential role of large scale climate variability is evaluated using indices of the El Niño Southern Oscillation (ENSO), Pacific Decadal Oscillation (PDO), Atlantic Multidecadal Oscillation (AMO), North Atlantic Oscillation (NAO), Arctic Oscillation, and East Atlantic pattern (EA). This approach is consistent with recent data driven studies investigating the modulation of regional extremes by large scale climate modes [29]. Full methodological details, preprocessing steps, analogue selection criteria, sensitivity analyses, statistical procedures, and data sources, including the National Oceanic and Atmospheric Administration Climate Prediction Center, Extended Reconstructed Sea Surface Temperature version 5 dataset, National Centers for Environmental Information, and Koninklijk Nederlands Meteorologisch Instituut Climate Explorer [30], are provided in the supplementary material.

We quantify socioeconomic exposure to temperature hazards enhanced by climate change by crossing event-day hazard masks with spatially gridded population and GDP data over North America domain. Population data are derived from the global human settlement layer for 2025 and regridded at 0.5° spatial resolution [31], and GDP per capita from a global gridded dataset at the same resolution [32]. The hazard is defined from detrended and deseasonalized temperature anomalies and restricted to areas where the ClimaMeter analysis shows a significant positive

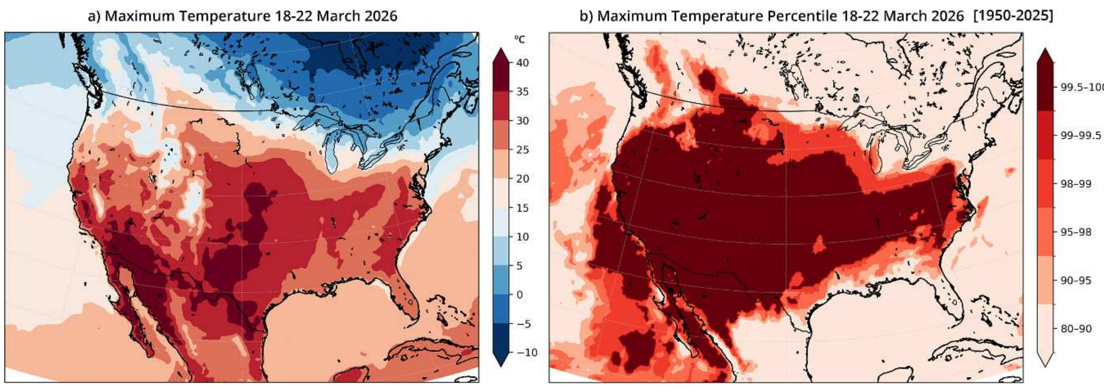

Figure 1. figure 1: (a) Maximum 2 m air temperature (°C) over the period 18–22 March 2026, based on ERA5 reanalysis. (b) Corresponding percentile of the 5 d maximum temperature relative to the 1950–2025 ERA5 climatology for the same calendar period.

temperature change. Three nested intensity levels (where intensity refers to the local magnitude of the temperature hazard relative to the grid-cell climatological distribution) are defined using the 0.98, 0.99, and 0.995 quantiles (moderate, severe, and extreme). Specifically, the moderate class includes hazard values between the 0.98 and 0.99 quantiles, the severe class includes values between the 0.99 and 0.995 quantiles, and the extreme class includes values above the 0.995 quantile. Exposure is computed by aggregating population and GDP within each class under present-day conditions (see [33] for complete explanation).

3. Event overview

The March 2026 heatwave was a record-breaking heat wave that affected several major cities in the southwestern United States, with temperatures far above seasonal averages [34]: (1) in Phoenix (AZ), temperatures reached about 38 °C, setting a new March record; (2) Las Vegas (NV) recorded around 34 °C, marking its highest March temperature ever; (3) in downtown Los Angeles (CA), temperatures climbed to approximately 35 °C, also breaking daily records; (4) even higher-elevation areas such as Flagstaff (AZ) experienced unusually high temperatures, reaching about 24 °C.

The spatial extent and persistence of the event are further highlighted in figures 1(a) and (b), which present the maximum temperature during the 18–22 March 2026 period and the corresponding percentile relative to the 1950–2025 ERA5 climatology. The 5 d maximum temperature field (figure 1(a)) confirms that large parts of the western and central North America experienced sustained anomalously high temperatures, with widespread values exceeding 30 °C–35 °C. What is particularly striking, however, is the extremeness of the event in a climatological context. As shown in figure 1(b), a vast contiguous area of the United States falls within the highest percentiles, with large regions exceeding the 99th percentile and extensive cores reaching the 99.5–100th percentile range. This indicates that, when considering the full 5 d period, the event ranks among the most extreme warm episodes on record for this time of year. This is also highlighted by figure 2(e), where temperature anomalies are shown. A very large warm anomaly covers much of the western and central United States, with a core broadly in the 10 °C–15 °C range above climatology. Positive anomalies extend well beyond the core into much of the central and southern North America. The heatwave was associated with a large-scale ridge (an extended region of positive z500 anomaly) over western and central North America. Figure 2(a) shows a broad positive z500 anomaly centred over the western to central United States, with values exceeding 200 m over the core of the ridge and extending over a large part of the continent. Negative anomalies are found to the north and northeast of the ridge, as well as over the northeastern Pacific side of the domain. This is a canonical configuration for widespread warm anomalies over the United States. Observed impacts include marked phenological anomalies across North America, with early vegetation activity indicating biosphere involvement and increased vulnerability to subsequent frost.

4. Results

4.1. Changes in hazard intensity

The ClimaMeter diagnostics for the March 2026 heatwave are shown in figure 2. The past and present analogue composites (figures 2(b) and (c)) both reproduce a broadly similar large-scale circulation structure. In both cases, the main positive z500 centre is located over the western to central United States. While the overall circulation pattern remains largely unchanged between the two composites, the difference between the present and past

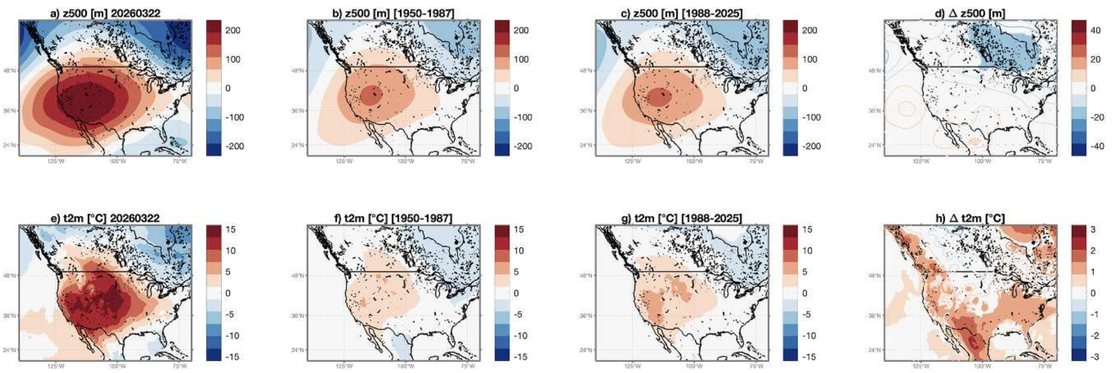

Figure 2. Z500 analogue attribution diagnostics for the March 2026 North America heatwave. Panels (a), (e) show the event day fields for the period 18–22 March 2026: z500 anomaly, 2 m temperature anomaly. Panels (b), (f) show the corresponding composite means for the past analogue period (1950–1987), while panels (c), (g) show the present analogue period (1988–2025). Panels (d), (h) show the present minus past differences.

circulation fields (figure 2(d)) highlights a statistically significant negative anomaly (up to −30 m) over the north-eastern portion of the domain. This feature suggests a slight weakening of geopotential heights in northern North America under present-day climate conditions, whereas no substantial changes are detected over the core region of the ridge. Overall, the comparison indicates that the dynamical configuration associated with the event remains broadly consistent between past and present analogues, with only limited regional differences. Figure 2(a) shows that the z500 anomaly pattern during the event exhibits higher positive values than those in either analogue composite. Examining the similarity between the event z500 anomaly map and its analogues (supplementary figure S1(q)) reveals that this similarity falls in the upper tail of the distribution, with respect to the self-similarity among the analogues themselves (for a detailed discussion of analogue quality, see [26]). This indicates that, while the event's circulation retains the spatial characteristics of a familiar ridge pattern, its exceptional intensity places it at the margins of what the observed record of analogues can represent. As a result, the analogue composites should not be interpreted as exact reconstructions of the March 2026 event, but rather as the closest available circulation-conditioned reference states within the ERA5 record. This limitation increases uncertainty in the quantitative representation of the event magnitude, but it does not affect the main conditional comparison between past and present analogue sets. The key inference is therefore that, for circulation patterns resembling the March 2026 ridge, present-day conditions are associated with substantially warmer near-surface temperatures than comparable past conditions.

The clearest attribution signal appears in near-surface temperature. The past analogue composite (figure 2(f)) already shows positive temperatures over the same broad region, but these are much weaker, with values generally around a few degrees above climatology and a much less intense core. The present analogue composite (figure 2(g)) remains similar in spatial structure to panel f, but is systematically warmer, more spatially extensive across the western and southern areas of the domain.

This difference is made explicit in figure 2(h). The present-minus-past 2 m temperature difference is positive over almost the entire North America region. The most common values appear to lie between about 1 °C and 3 °C, with locally higher values over parts of the western and southern United States and not significant differences across large parts of the Central regions. The signal is broad and spatially coherent. Importantly, there are almost no large-scale regions of cooling over the continental United States. This is the strongest evidence in figure 2 that anthropogenic climate change amplified the thermal intensity of the event. A comparison with the mean climatological 2 m temperature change between the present and past periods over March–June (supplementary figure S13) shows a broadly similar spatial pattern and magnitude, indicating that the analogue-based warming signal is consistent with the regional background thermodynamic warming.

We also observe upper-level winds strengthening and slight reorganization of the midlatitude jet over North America in the recent period (supplementary figure S14). Concurrently, low-level relative humidity (supplementary figure S15) exhibits a widespread increase, particularly over the southwestern United States. Vertical profiles (supplementary figure S16) further indicate enhanced near-surface moisture, especially in coastal regions, consistent with a more humid lower troposphere.

4.2. Seasonality and natural variability

The diagnostics in figure 3 provide complementary information on the timing of analogue occurrence and the role of large scale climate variability.

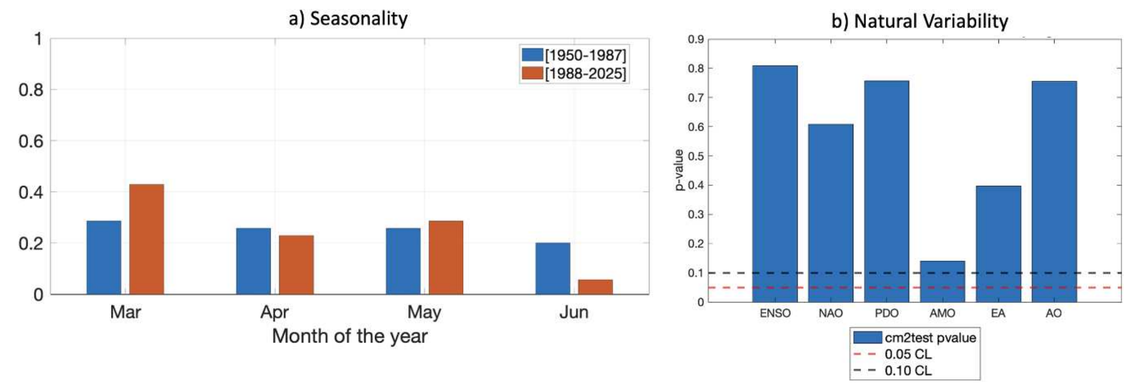

Figure 3. Seasonality and natural variability diagnostics for the March 2026 heatwave. Panel (a) shows the monthly frequency of analogue occurrence in the past (1950–1987) and present (1988–2025) periods. Panel (b) reports p values from a Cramér–von Mises test comparing the distributions of major climate indices between analogue sets, with reference lines at the 0.05 and 0.10 levels.

Panel (a) shows the seasonal distribution of analogue occurrences in the past (1950–1987) and present (1988–2025) periods, with the analysis restricted to the extended spring season (March–June; the corresponding 12 month configuration is reported in the supplementary material as a sensitivity test). In the present climate, the events are clustered mainly in March, with smaller contributions from April and May. In contrast, under the past climate, the distribution is more evenly spread throughout the season. The largest differences are observed in March and June: factual analogues are more concentrated in the early part of the season, whereas counterfactual analogues occur more frequently in the later part. Secondary contributions from the winter months (December–February), more pronounced in the past period, are visible in the 12 month configuration (supplementary figure S4) and are consistent with the late-winter/early-spring character of the event. Taken together, these results indicate that the March 2026 event belongs to a late-winter to mid-spring regime that is dynamically distinct from summer heat extremes over the region—consistent with the absence of summer analogues in both configurations—and that, between the past and present periods, the analogue distribution has shifted towards earlier calendar dates by approximately one month. This earlier-season shift is potentially significant from an impact perspective, as societies and ecosystems are typically less prepared for extreme heat occurring outside the conventional warm season.

Panel (b) reports p-values from a Cramér–von Mises test comparing the distributions of the ENSO, NAO, PDO, AMO, EA, and Arctic oscillation indices between the past and present analogue sets, with horizontal reference lines at the 0.05 and 0.10 significance levels. In the reference configuration, all the climate variability indexes have p-values above 0.10.

These results should be interpreted alongside the sensitivity analyses reported in the supplementary materials, which assess the stability of each mode under variations in the analogue-selection threshold (20, 35, and 60 analogues) and in the analysis setup (reference configuration, shorter period, smaller search domain, and full 12 month pool). Across these tests, the identified modes generally do not exhibit significant differences, with the exceptions of the NAO in the full 12 month pool experiment and the PDO in the shorter-period sensitivity test. These discrepancies can plausibly be explained by the characteristics of the respective modes. Including the full annual cycle may introduce a stronger influence of the NAO, which is most pronounced during winter, whereas reducing the analogue search period by approximately one decade may affect the representation of the PDO, given its variability on longer timescales. Taken together, these findings suggest that natural variability plays only a limited role in shaping the differences between the two periods, which can therefore be largely attributed to anthropogenic climate change. Accordingly, the large-scale, spatially coherent warming signal in 2 m temperature observed between past and present analogues remains robust across all sensitivity configurations and can be interpreted as evidence of thermodynamic amplification driven by anthropogenic climate change.

4.3. Socioeconomic exposure to climate intensified heat

Figure 4 shows the exposure analysis for population and GDP. In panels (a) and (c), the gre yscale background gives the spatial distribution of population and GDP, while the coloured overlays identify the areas where the temperature hazard coincides with a statistically significant positive ClimaMeter signal. The three nested classes are shown as orange for moderate (98th percentile), red for severe (99th percentile) and purple for extreme (99.5th percentile).

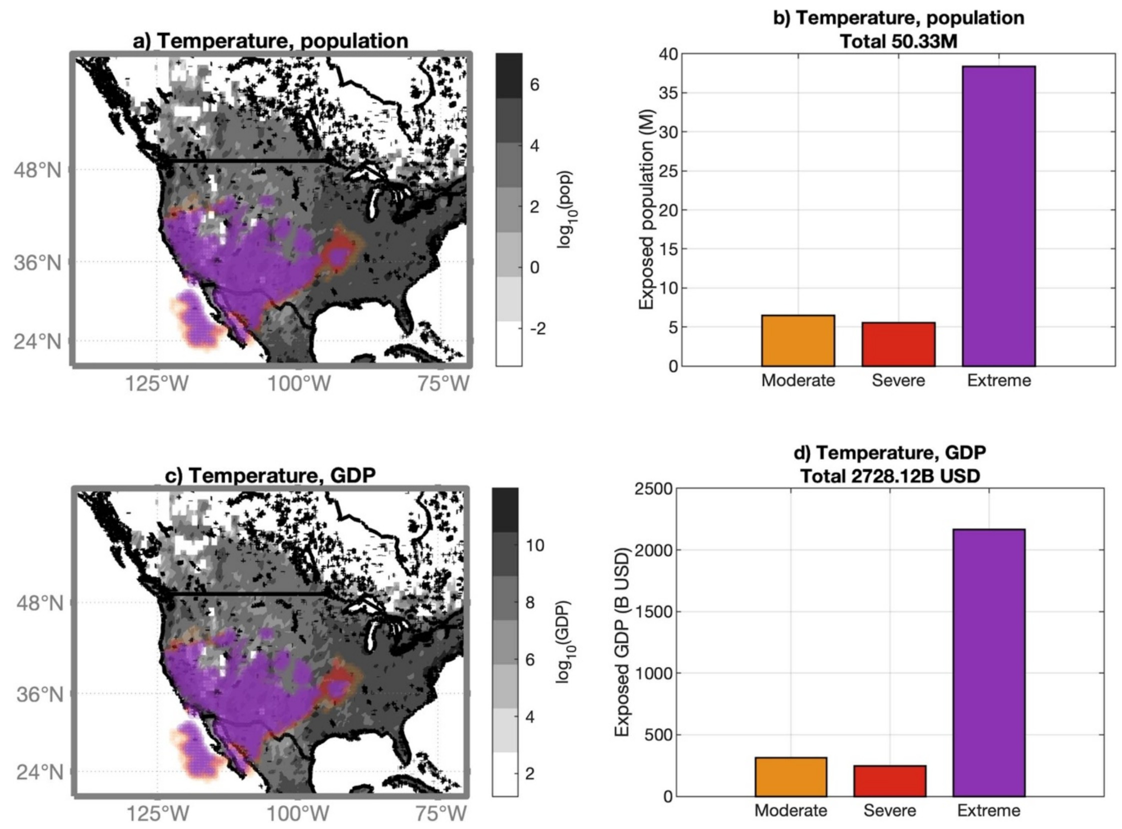

Figure 4. Socioeconomic exposure to climate-intensified temperature hazards during the March 2026 North America heatwave. Panels (a) and (c) show the spatial distribution of population and GDP in greyscale, respectively. In both panels, the same hazard overlay is shown, representing three nested temperature hazard intensity classes: moderate (orange, values between the 0.98 and 0.99 quantiles), severe (red, values between the 0.99 and 0.995 quantiles), and extreme (purple, values above the 0.995 quantile). Only areas where the heat hazard overlaps with a statistically significant positive temperature change in the ClimaMeter analysis are retained. Panels (b) and (d) show the corresponding totals of exposed population and exposed GDP. In both cases, the extreme class dominates total exposure.

The first striking feature is the size of the extreme hazard footprint (figure 4(a)). The area experiencing extreme temperatures covers a vast region extending from the southwestern United States across the central states and toward the western side of the Mississippi basin. It is surprising that it is not just a small inner core surrounded by broad lower intensity rings. On the contrary, it occupies most of the attributed hazard region. The moderate and severe classes are visible mainly as thinner outer bands around the extreme class region, together with a few patches over the Southwest and Mexico. This geometry already suggests that the total exposure is dominated by the extreme class.

The population bar chart (figure 4(b)) shows that of the total exposed population of 50.33 million people, the extreme class accounts for roughly 37 million, whereas the moderate and severe classes each contribute only around 6 million. This means that about 74% of all exposed population lies in the extreme class. This is an important result. It means that the event did not simply produce a broad region of modest climate amplified heat. Instead, most of the exposed population was located where the heat hazard exceeded the highest threshold considered here.

The GDP exposure (figure 4(d)) is even more concentrated. Among the total exposed GDP of 2728.12 billion USD, the extreme class represents more than 2000 billion USD, while the moderate and severe classes are each below 500 billion USD. The economic exposure therefore has the same structure as the population exposure, but with an even stronger dominance of the extreme class. This indicates that the strongest climate amplified heat overlapped not only with populous areas, but also with highly productive parts of the United States economy.

The exposure maps also show that the large exposure totals are not due solely to the broad spatial extent of the hazard. Although large portions of the western United States are affected, the highest totals arise because the heat footprint extends into central and southern regions characterized by substantial population density and economic activity. In this sense, the March 2026 event combined three relevant features: large spatial extent, a strong and statistically detectable warming signal, and substantial overlap with present-day socioeconomic assets.

These exposure estimates should be interpreted as indicators of spatial coincidence between hazard and socioeconomic assets rather than as direct measures of realized impacts. The analysis is based on static present-day population and GDP fields aggregated on the study grid and therefore does not account for sub-grid urban structure, transient population movements, differential vulnerability, infrastructure sensitivity, adaptation capacity, or the fraction of economic activity effectively disrupted by heat. GDP exposure in particular should not be interpreted as actual economic loss.

Overall, figure 4 shows that the exposure associated with this event is overwhelmingly concentrated in the most intense class of climate amplified heat. This strengthens the interpretation that the event represented not just a widespread warm anomaly, but a very severe heat hazard across a large and socioeconomically important part of the United States.

4.4. Discussion

The ERA5-based ClimaMeter analysis indicates that anthropogenic climate change amplified the thermal hazard associated with the March 2026 heatwave over North America. The event developed in association with a strong upper-level ridge over western and central North America. From a dynamical perspective, ridge-like circulation patterns of similar structure are identified in both the past and present analogue periods; however, the z500 anomaly intensity during the event itself exceeds that of both analogue composites making this pattern exceptional. The key difference between the two climate periods lies in the near-surface temperatures associated with analogous circulation states. Present-day analogues are systematically warmer than past analogues across the southwestern regions of North America, generally by about 1 °C - 3 °C and locally more.

Natural variability had a limited contribution to the exact circulation setting of the event. The analogue distributions do not differ significantly for all the modes. These results suggest a primary role of climate change, indicating that similar large-scale circulation patterns now yield substantially warmer conditions than they did in the mid twentieth century.

The exposure analysis further shows that a very large present-day population and a very large amount of present-day economic activity were located in areas where the heat hazard coincided with a statistically significant warming signal. Exposure is dominated by the extreme class, both for population and GDP. The event therefore provides a clear example of how anthropogenic climate change can amplify not only thermal hazard itself, but also the amount of society exposed to the strongest part of that hazard.

4.5. Limitations

The framework remains conditional on circulation similarity. It does not use dedicated anthropogenic external-forcing experiments and does not estimate the unconditional probability of the event in a counterfactual climate. Conditioning on dynamically analogous configurations removes much of the dynamical contribution, so that the period-to-period difference in temperature reflects predominantly the thermodynamic response to a warmer background climate. The ClimaMeter analysis should therefore not be read as a standalone formal attribution of the March 2026 heatwave to anthropogenic forcing; it detects a change between a cooler past climate and the present rather than separating anthropogenic forcing from internal variability. Taken on its own, it is one line of evidence. It can, however, be combined with others: the World Weather Attribution assessment [25], which uses observations and climate-model simulations to estimate changes in event likelihood and intensity; regional trend and event studies; and the well-established thermodynamic expectation that a warmer atmosphere raises the temperatures associated with a given circulation pattern. Combined with these, the present analysis contributes to a coherent and physically consistent, albeit conditional, attribution statement. The convergence of these independent lines of evidence is what licenses an attribution conclusion; the conditional circulation-analogue estimate presented here is complementary to, and reinforced by, the probabilistic assessment.

The significance assessment is pointwise and does not explicitly correct for multiple testing across the spatial field. The broad coherence of the positive temperature signal supports the interpretation of the main pattern, but isolated small-scale features should be treated cautiously. The natural variability diagnostics are also indicative rather than mechanistic. The p values in figure 3 identify modes that do not differ between analogue sets, but they do not establish causal pathways linking those modes to event magnitude.

The hazard intensity classification relies on quantile-based cut-offs of the detrended and deseasonalized temperature anomaly distribution at the 0.98, 0.99 and 0.995 quantiles for the moderate, severe and extreme classes. No unique physically prescribed threshold exists, and any partition of the upper tail involves a modelling choice. The selected thresholds are internally consistent because their exceedance probabilities $\{0.02, 0.01, 0.005\}$ form a geometric progression, their spacing is close to uniform on the natural tail scale $\tau = -\log_{10}(1-q)$, as expected under Pickands–Balkema–de Haan asymptotic behaviour and the highest threshold retains enough grid points for stable population- and GDP-weighted aggregation. Alternative thresholds, including 0.95/0.99/0.999 or return-period-based definitions, would change absolute exposure values and class shares. The qualitative ranking moderate $<$ severe $<$ extreme and the main exposure hotspots are expected to remain stable because they follow from the monotonic structure of the anomaly field. A systematic sensitivity analysis to threshold choice is left for future work.

The exposure analysis uses static present-day population and GDP datasets aggregated to the analysis grid. It does not resolve sub-grid urban heterogeneity, temporary population movements, demographic vulnerability, infrastructure sensitivity, behavioural responses, or adaptation measures. Exposure should therefore be interpreted as the spatial coincidence between the hazard and socioeconomic assets, not as realized human or economic impacts. GDP does not measure economic activity disrupted by heat and should not be interpreted as economic loss. Future developments could include dynamic population datasets, evolving socioeconomic exposure, vulnerability indicators, sector-specific economic metrics, infrastructure layers, and impact observations such as excess mortality, labor productivity losses, energy demand, or insured damages. Comparing exposure across historical periods would also help separate the roles of changing hazard, demographic evolution, and socioeconomic development. The supplementary information shows that the main spatial patterns remain similar when neighboring quantile thresholds are adopted or when the area, analogue-search periods and seasonality are changed, increasing confidence in the robustness of the exposure estimates.

5. Conclusion

We applied the ClimaMeter analogue based attribution protocol to the March 2026 United States heatwave and complemented the meteorological analysis with a population and GDP exposure assessment. The event was associated with a strong ridge over western and central North America and exceptionally large positive near-surface temperature anomalies across southern and western regions of the United States. Comparing present day and past analogue sets shows that similar circulation patterns now produce substantially warmer conditions than in the cooler past climate, with widespread positive differences in 2 m temperature of roughly 1 to 3 °C and locally larger values. The results are compatible with the World Weather Attribution framework [25], highlighting that such an event would have been extremely unlikely in a pre-industrial climate.

The exposure analysis shows that this amplification overlapped with very large present-day socioeconomic assets. A total of 50.33 million people and 2728.12 billion USD in GDP were located in areas where the event coincided with a statistically significant positive temperature change signal, and most of this exposure fell in the most extreme class. The March 2026 heatwave therefore illustrates a now recurrent pattern in North America: persistent ridging remains the immediate dynamical driver of extreme heat, but anthropogenic warming substantially increases the temperatures reached under such circulation states and thereby increases the scale of exposure.

Acknowledgments

We acknowledge funding from the European Union's Horizon 2020 research and innovation programme under Grant Agreements Nos. 101003469 (XAIDA), the ANR Project PowDev (Strategic Development of the Power Grids of the Future, ANR-22-PETA-0016), the ANR Project Templex (ANR-23-CE56-0002), the ANR Project TRACCS-PC4-EXTENDING (ANR-22-EXTR-0005), and the Swedish Research Council Vetenskapsrådet (2022-06599).

Data availability statement

The data that support the findings of this study are openly available at the following URL/DOI: https://cds.climate.copernicus.eu/datasets/reanalysis–era5–single–levels?tab=overview [27].

Supplementary Material available at https://doi.org/10.1088/1748-9326/ae870d/data1.

Competing interest

The authors declare no competing interests nor conflicts of interest. No human or animal data have been used in this study.

Author contributions

Davide Faranda 0000-0001-5001-5698
Conceptualization (lead), Data curation (lead), Formal analysis (lead), Funding acquisition (lead), Investigation (lead), Methodology (lead), Project administration (lead), Resources (lead), Software (lead), Supervision (lead), Validation (lead), Visualization (lead), Writing – original draft (lead), Writing – review & editing (lead)

Marco Zanchi 0000-0003-4847-9367
Conceptualization (lead), Data curation (lead), Formal analysis (lead), Investigation (lead), Methodology (lead), Validation (lead), Visualization (lead), Writing – original draft (lead), Writing – review & editing (lead)

Pascal Yiou 0000-0001-8534-5355
Methodology (supporting), Writing – original draft (supporting), Writing – review & editing (supporting)

Marco Chericoni 0000-0002-8078-6933
Writing – original draft (supporting), Writing – review & editing (supporting)

Mathieu Vrac
Methodology (supporting), Writing – original draft (supporting), Writing – review & editing (supporting)

Haosu Tang 0000-0002-2924-0126
Writing – original draft (supporting), Writing – review & editing (supporting)

Stavros Dafis 0000-0002-1513-1930
Formal analysis (supporting), Visualization (supporting), Writing – original draft (supporting), Writing – review & editing (supporting)

Gianmarco Mengaldo 0000-0002-0157-5477
Methodology (supporting), Writing – original draft (supporting), Writing – review & editing (supporting)

Tommaso Alberti 0000-0001-6096-0220
Conceptualization (supporting), Formal analysis (supporting), Funding acquisition (supporting), Methodology (supporting), Visualization (supporting), Writing – original draft (supporting), Writing – review & editing (supporting)

References

[1] Seneviratne S I *et al* 2021 *Weather and Climate Extreme Events in a Changing Climate Climate Change 2021: The Physical Science Basis. Contribution of Working Group I to the Sixth Assessment Report of the Intergovernmental Panel on Climate Change*, eds V Masson-Delmotte *et al* (Cambridge University Press) pp 1513–766
[2] Gutiérrez J M *et al* 2021 *Atlas Climate Change 2021: The Physical Science Basis* eds V Masson-Delmotte *et al* (Cambridge University Press) pp 1927–2058
[3] García-Martínez I M and Bollasina M A 2021 *Environ. Res. Lett.* **16** 094039
[4] Quilcaille Y *et al* 2025 *Nature* **645** 392–8
[5] Perkins-Kirkpatrick S and Lewis S 2020 *Nat. Commun.* **11** 3357
[6] Domeisen D I, Eltahir E A, Fischer E M, Knutti R, Perkins-Kirkpatrick S E, Schär C, Seneviratne S I, Weisheimer A and Wernli H 2023 *Nat. Rev. Earth Environ.* **4** 36–50
[7] Suarez-Gutierrez L, Muller W A, Li C and Marotzke J 2020 *Clim. Dyn.* **55** 429–47
[8] Chen K, Boomsma J and Holmes H A 2023 *Sci. Rep.* **13** 9570
[9] Zhang X, Zhou T, Zhang W, Ren L, Jiang J, Hu S, Zuo M, Zhang L and Man W 2023 *Nat. Commun.* **14** 1690
[10] Bartusek S, Kornhuber K and Ting M 2022 *Nat. Clim. Change* **12** 1143–50
[11] Thompson V, Kennedy-Asser A T, Vosper S, Lo Y Y, Huntingford C, Andrews M B, Collins M and Mitchell D 2022 *Sci. Adv.* **8** eabm6860
[12] White R H E A 2023 *Nat. Commun.* **14** 727
[13] Fleishman E, Rupp D E, Loikith P C, Bumbaco K A and O'Neill L W 2025 *Bull. Am. Meteorol. Soc.* **106** E1155–74
[14] Philip S *et al* 2022 El: rapid attribution analysis of the extraordinary heat wave on the pacific coast of the us and canada in june 2021 *Earth Syst. Dynam.* **13** 1689–713
[15] Lopez H, Lee S K, West R, Kim D and Jia L 2025 *Nat. Commun.* **16** 6544
[16] Dong C *et al* 2024 *Nat. Geosci.* **17** 979–86
[17] Matthews T, Raymond C, Foster J, Baldwin J W, Ivanovich C, Kong Q, Kinney P and Horton R M 2025 *Nat. Rev. Earth Environ.* **6** 193–210
[18] Anderson G B and Bell M L 2010 *Environ. Health Perspect.* **119** 210
[19] Howard J T, Androne N, Alcover K C and Santos-Lozada A R 2024 *JAMA* **332** 1203–4
[20] Narayanan A and Keellings D 2025 *PLOS Clim.* **4** e0000610
[21] Liu Z, Anderson B, Yan K, Dong W, Liao H and Shi P 2017 *Sci. Rep.* **7** 43909
[22] Dong J, Peng J, He X, Corcoran J, Qiu S and Wang X 2020 *Landsc. Urban Plan.* **203** 103907
[23] Yoo E H, Eum Y, Roberts J E, Gao Q and Chen K 2021 *Sci. Total Environ.* **792** 148246
[24] Qu Y, Zhang W, Boutelle A Y M, Ryan I, Deng X, Liu X and Lin S 2023 *Am. J. Kidney Dis.* **81** 353–62
[25] World Weather Attribution 2026 Record-shattering march temperatures in western north america virtually impossible without climate change (available at: www.worldweatherattribution.org/record-shattering-march-temperatures-in-western-north-america-virtually-impossible-without-climate-change/)
[26] Faranda D *et al* 2024 *Weather Clim. Dyn.* **5** 959–83
[27] Hersbach H *et al* 2020 *Q. J. R. Meteorol. Soc.* **146** 1999–2049
[28] Efron B and Tibshirani R J 1993 An Introduction to the Bootstrap *Monographs on Statistics and Applied Probability* (Chapman and Hall)
[29] Faranda D *et al* 2025 *Phys. Rev. E* **111** 064209
[30] de Bilt:Koninklijk Nederlands Meteorologisch Instituut 2022 Knmi climate (available at: explorerhttps://climexp.knmi.nl/start.cgi) (Accessed 17 November 2025)
[31] Schiavina M *et al* 2022 *Publications Office of the European Union* (Luxembourg)
[32] Kummu M, Taka M and Guillaume J H 2018 *Sci. data* **5** 1–15
[33] Faranda D, Messori G, Alvarez-Castro C and Bourdin S 2026 *Environ. Res.* 16 094039
[34] NOAA NESDIS 2026 Noaa's goes west watches record heat wave (available at: www.nesdis.noaa.gov/news/noaas-goes-west-watches-record-heat-wave) (Accessed 26 March 2026)